JOURNAL OF MATERIALS SCIENCE 32 (1997) 633–641

Stress transfer in the fibre fragmentation test

Part III *Effect of matrix cracking and interface debonding*

H.-Y. LIU, Y.-W. MAI*, L. YE, L.-M. ZHOU
Centre for Advanced Materials Technology, Department of Mechanical and Mechatronic Engineering, The University of Sydney, Sydney, New South Wales 2006, Australia

A theoretical stress analysis has been developed for the fibre fragmentation test in the presence of matrix cracks at sites of fibre breaks. The strain energy release rates for both matrix cracking and interface debonding are calculated for a carbon fibre/epoxy matrix composite. By comparing these strain energy release rates with the corresponding specific fracture resistances, the competition between matrix crack growth and interface debonding has been studied. The distributions of fibre axial stress and interfacial shear stress obtained from the present analysis show that the matrix crack substantially reduces the efficiency of stress transfer from the matrix to the fibre.

1. Introduction

The fibre fragmentation test is now commonly used to study the fibre/matrix interfacial properties and stress transfer in fibre composite materials. The test involves a single fibre embedded completely in a matrix that is subjected to an axial tension. Load is transferred from the matrix to the fibre by the interfacial shear stress. As the applied stress increases, the fibre breaks into smaller fragments. This process continues until the axial stress induced in the fibre fragment is no longer capable of producing further rupture, which is referred to as the saturation stage. The maximum fibre fragment length obtained at the saturation stage is called the critical transfer length (CTL). Early investigation by Kelly and Tyson [1] provided a simple formula to correlate the critical transfer length with the average interfacial shear strength, τ, i.e.

$$CTL = \frac{\sigma_{fs}^{*} d}{2\tau} \quad (1)$$

where σ_{fs}^{*} is the fibre tensile strength at the critical length (CTL) and d the fibre diameter. The major underlying assumptions of this model are that the matrix behaviour is rigidly perfectly plastic and the fragment lengths at the saturation stage are uniformly distributed. A modified formula has been proposed

$$\tau = K \frac{\sigma_{fs}^{*} d}{2L} \quad (2)$$

where L is the mean fibre fragment length and the non-dimensional correction factor K is used to take into account the variation in the fragment length. If the fibre fragment length is assumed to vary uniformly between 0.5 CTL and CTL, $K = 0.75$ [2]. In addition, a statistical model has been used to describe the fragmentation behaviour [3, 4] and K is related to the Weibull modulus of the fibre strength distribution.

Contrary to the conventional assumptions that the fibre/matrix interface is either perfectly bonded or completely debonded, several analytical models [5, 6] have been developed to study stress transfer in the fibre fragmentation test considering that both bonded and debonded regions exist simultaneously along the interface. A new fracture mechanics-based debonding criterion at the fibre/matrix interface has been recently proposed [6]. In a recent paper, Liu *et al.* [7] also presented a computer simulation study of the fibre fragmentation test. Fibre breakage is assumed to be controlled by pre-existing flaws on the fibre surface when the fracture toughness is exceeded. From the debonding criterion [6], numerical results of the mean fibre fragment length and mean fibre debond length versus applied stress, as affected by the distribution of the pre-existing flaws, have been calculated for a carbon fibre/epoxy matrix composite.

A noteworthy phenomenon in the fibre fragmentation test, which has been mentioned by many researchers [8–13], is that a small circular matrix crack often appears around a fibre break (Fig. 1). As the fibre breaks, a high stress concentration is exerted on the surrounding matrix, which initiates a small matrix crack. When the applied stress is increased, the matrix crack may propagate outwards. Alternatively, an interfacial debond may start along the fibre/matrix interface. Both matrix crack propagation and interface debonding have been observed in the fibre fragmentation test. Two important questions arise: (i) what governs the competition between matrix cracking and interface debonding, and (ii) how does the matrix crack affect the stress transfer from the matrix to the fibre? Gent and Wang [12, 13] investigated the fracture behaviour of resin cracking by both finite-element analysis and experiments. It was found that even for the samples with perfect adhesion between the matrix

*Author to whom all correspondence should be addressed.

0022–2461

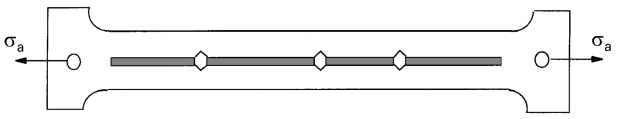

Figure 1 A schematic illustration of a fibre fragmentation test specimen.

resin and fibre, interfacial failure would occur if the fibre radius was less than about one-fifth the matrix cylinder radius. For the fibres of large radius, either fibre pull-out or matrix cracking can take place, the competition depends on the relative levels of interfacial fracture energy and fracture resistance of the matrix resin. But the effect of the matrix crack on the stress transfer was not discussed in their work.

The aim of the current work is to present a theoretical analysis of the fibre fragmentation test in the presence of a matrix crack. The stress distributions in the fibre, matrix and interface are obtained from the axisymmetrical cylindrical single fibre composite model. The strain energy release rates for both the matrix crack and the interface crack are calculated for a carbon fibre/epoxy matrix composite. Using the minimum fracture stress criterion the competition between matrix cracking and interface debonding is discussed in terms of the fibre radius and elastic modulus of the matrix. The effects of thermal residual stress in both radial and axial directions are also included in this model. (In the debonded region, because the thermal residual stress in the axial direction is absent, the thermal residual stress in the radial direction is expressed by q_0 which is caused by ΔT, (in this work q_0 is the experimental datum [6]). In the bonded region, the radial stresses σ_f^r, σ_{m1}^r and σ_{m2}^r are functions of the axial stresses σ_f^z, σ_{m1}^z and σ_{m2}^z (Appendix A) which are dependent on ΔT. So in both the debonded and bonded regions, σ_f^r, σ_{m1}^r and σ_{m2}^r are dependent on ΔT.)

2. Basic equations

2.1. Stress transfer

To study the stress transfer from the matrix to the fibre, a fragment of length $2L$ with two initial partially debonded regions of length $2l$ is taken as a mechanics model (Fig. 2). A fibre of radius a is embedded in a matrix cylinder with radius R. Two initial co-axial matrix cracks of radius b are present at both ends of the fragment. For simplicity, it is assumed that both matrix cracks have the same radius. A set of the cylindrical coordinates (r, θ, z) is selected as shown in Fig. 2. The average tensile stress, σ, caused by the remote applied stress, σ_a, at each end of the model is given by

$$\sigma = \frac{\sigma_a R^2}{R^2 - b^2} \tag{3}$$

Because of the very small radius of the matrix crack and small area of the disturbed stress field, this average stress is used as a boundary condition for the study of stress transfer in the fragment.

In a fibre/matrix fragment, the fibre is embedded in a relatively large matrix and a uniform load is applied

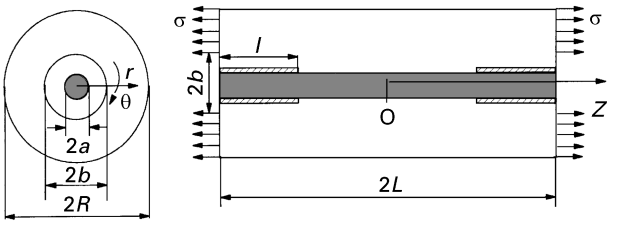

Figure 2 A single-fibre model composite with matrix cracks and partial debonding at the two ends of the fibre fragment.

to each end of the matrix. In most areas of the matrix, the axial stress can be considered independent of coordinate r. So a basic assumption used here is that the axial stresses are functions of coordinate z only. The boundary conditions at the two ends of this model are given by

$$\sigma_f^z(z = \pm L) = 0 \qquad (0 \leqslant r \leqslant a) \tag{4a}$$

$$\sigma_m^z(z = \pm L) = 0 \qquad (a \leqslant r \leqslant b) \tag{4b}$$

$$\sigma_m^z(z = \pm L) = \sigma \qquad (b \leqslant r \leqslant R) \tag{4c}$$

where the superscript denotes the coordinate direction and subscripts f and m refer to fibre and matrix respectively. The matrix may be divided into two regions: matrix (m1) $(b \leqslant r \leqslant R)$ and matrix (m2) $(a \leqslant r \leqslant b)$. Therefore, together with the fibre, a three-concentric-cylinder model is obtained. The equilibrium conditions are

$$\frac{d\sigma_f^z}{dz} = -\frac{2}{a}\tau_a \tag{5a}$$

$$\frac{d\sigma_{m1}^z}{dz} = \frac{2b}{R^2 - b^2}\tau_b \tag{5b}$$

$$\frac{d\sigma_{m2}^z}{dz} = \frac{2}{b^2 - a^2}(a\tau_a - b\tau_b) \tag{5c}$$

where τ_a and τ_b are the shear stresses at the interfaces $r = a$ and $r = b$, respectively. The equilibrium equation between the axial stress and shear stress in each cylinder in the z direction is

$$\frac{d\sigma^z}{dz} + \frac{\partial\tau^{rz}}{\partial r} + \frac{\tau^{rz}}{r} = 0 \tag{6}$$

Therefore, in conjunction with Equations 5a–c we have

$$\tau_{m1}^{rz} = \frac{b}{R^2 - b^2}\left(\frac{R^2}{r} - r\right)\tau_b \tag{7a}$$

$$\tau_{m2}^{rz} = \frac{1}{b^2 - a^2}\left[ab(b\tau_a - a\tau_b)\frac{1}{r} + (b\tau_b - a\tau_a)r\right] \tag{7b}$$

For this fibre/matrix system, the radial displacement gradient with respect to the z-direction is ignored compared to the axial displacement gradient with respect to the r-direction [14], the shear stress can be approximately expressed as

$$\tau^{rz} = \frac{E_m}{2(1 + \nu_m)}\frac{\partial u^z}{\partial r} \tag{8}$$

where u^z is the displacement in the z direction E and ν are Young's modulus and Poisson's ratio, respectively.

Combining Equations 7a, b and 8 and integrating for each cylinder gives

$$\frac{E_m}{2(1+\nu_m)}[u^z_{m1}(R,z)-u^z_{m1}(b,z)] = \frac{b}{R^2-b^2}\left(R^2\ln\frac{R}{b}-\frac{R^2-b^2}{2}\right)\tau_b \quad (9a)$$

$$\frac{E_m}{2(1+\nu_m)}[u^z_{m2}(b,z)-u^z_{m2}(a,z)] = \frac{1}{b^2-a^2}\left[ab(b\tau_a-a\tau_b)\ln\frac{b}{a}+(b\tau_b-a\tau_a)\frac{b^2-a^2}{2}\right] \quad (9b)$$

The relationships between the axial strain, displacement and stress are given by

$$\varepsilon^z(r,z) = \frac{\partial u^z}{\partial z} = \frac{1}{E}\{\sigma^z-\nu[\sigma^r(r,z)+\sigma^\theta(r,z)]\}+\alpha^T\Delta T \quad (10)$$

where $\alpha^T\Delta T$ is the axial thermal residual strain and α^T is the coefficient of thermal expansion, ΔT the temperature change. The relationships between the radial, tangential and axial stresses are shown in Appendix A. Equilibrium of the fragment requires

$$\sigma^z_{m2} = \frac{1}{(b^2-a^2)}[(R^2-b^2)(\sigma-\sigma^z_{m1})-a^2\sigma^z_f] \quad (11)$$

In the debonded region ($L-l\leqslant z\leqslant L$ and $-L\leqslant z\leqslant -(L-l)$), frictional slip occurs along the debonded length (at $r=a$) and the shear stress τ_a is governed by Coulomb's friction law for a constant friction coefficient, μ, so that

$$\tau_a = -\mu(q_0+q^*) \quad (12)$$

where q_0 is the thermal residual clamping stress (compressive) in the radial direction [6]. q^* ($\sigma^r_f(a,z)$) is the additional radial stress at the interface arising from the differential Poisson contraction between the fibre and matrix when the matrix is subjected to an axial tension and is given in Appendix A.

At the interface $r=b$, the continuity of axial strains requires

$$\varepsilon^z_{m2}(b,z) = \varepsilon^z_{m1}(b,z) \quad (13)$$

Combining Equations 5a, 11 and 12 yields

$$\frac{d\sigma^z_f}{dz} = \eta_{11}\sigma^z_f+\eta_{12}\sigma^z_{m1}+\eta_{13}(\sigma+\bar\sigma) \quad (14a)$$

Differentiation of Equation 9a with respect to z and combining with Equations 5b, 10 and 11 gives

$$\frac{d^2\sigma^z_{m1}}{dz^2} = \eta_{22}\sigma^z_{m1}+\eta_{23}\sigma \quad (14b)$$

where

$$\bar\sigma = \frac{q_0}{k_{3A}}\frac{b^2-a^2}{R^2-b^2} \quad (15)$$

and the parameters K_{3A} and η_{ij} are given in Appendices A and B.

From the boundary conditions at two ends of the fragment, Equations 4a–c, the solutions of the axial stresses of the fibre and matrix in the debonded region are given by

$$\sigma^z_f = \frac{\eta_{12}B^*_1}{\eta^2_{11}-\eta_{22}}[(\eta_{11}\cosh\eta^{1/2}_{22}L+\eta^{1/2}_{22}\sinh\eta^{1/2}_{22}L)\times e^{-\eta_{11}(L-z)}-\eta_{11}\cosh\eta^{1/2}_{22}z-\eta^{1/2}_{22}\sinh\eta^{1/2}_{22}z)] -\frac{1}{\eta_{11}}\left[\left(\eta_{13}-\frac{\eta_{12}\eta_{23}}{\eta_{22}}\right)\sigma+\eta_{13}\bar\sigma\right]\times(1-e^{-\eta_{11}(L-z)}) \quad (16a)$$

$$\sigma^z_{m1} = B^*_1\cosh\eta^{1/2}_{22}z-\frac{\eta_{23}}{\eta_{22}}\sigma \quad (16b)$$

where

$$B^*_1 = \frac{1+(\eta_{23}/\eta_{22})}{\cosh\eta^{1/2}_{22}L}\sigma \quad (17)$$

In the bonded region ($-(L-l)\leqslant z\leqslant L-l$), the axial strains are required to be continuous at the interface between the fibre and matrix region m2 ($r=a$), that is

$$\varepsilon^z_f(a,z) = \varepsilon^z_{m2}(a,z) \quad (18)$$

Differentiating Equations 9a and b with respect to z and combining with Equations 5a–c, 10, 11, 13 and 18 gives the following differential equations for the axial stresses of fibre and matrix

$$\frac{d^2\sigma^z_f}{dz^2} = \lambda_{11}\sigma^z_f+\lambda_{12}\sigma^z_{m1}+\lambda_{13}\sigma-\lambda_{14}\sigma^T \quad (19a)$$

$$\frac{d^2\sigma^z_{m1}}{dz^2} = \lambda_{21}\sigma^z_f+\lambda_{22}\sigma^z_{m1}+\lambda_{23}\sigma \quad (19b)$$

where the parameters λ_{ij} are given in Appendix C. σ^T is an additional stress caused by axial thermal residual stress and is given by

$$\sigma^T = E_m\Delta T\,\alpha^T_m\left(1-\frac{\alpha^T_f}{\alpha^T_m}\right) \quad (20)$$

Solving Equations 19a and b with the boundary conditions gives the solutions of the axial stresses of fibre and matrix in the bonded region

$$\sigma^z_f = \frac{1}{\lambda_{21}}[B^*(r^2_1-\lambda_{22})\cosh r_1z+D^*(r^2_2-\lambda_{22})\cosh r_2z+\lambda_f\sigma-\lambda_{22}\lambda_T\sigma^T] \quad (21a)$$

$$\sigma^z_{m1} = B^*\cosh r_1z+D^*\cosh r_2z+\lambda_m\sigma+\lambda_T\sigma^T \quad (21b)$$

in which r_1, r_2 are given in Appendix C and

$$\lambda_f = \frac{\lambda_{21}(\lambda_{22}\lambda_{13} - \lambda_{12}\lambda_{23})}{\lambda_{12}\lambda_{21} - \lambda_{11}\lambda_{22}} \quad (22a)$$

$$\lambda_m = -\frac{\lambda_{21}\lambda_{13} - \lambda_{11}\lambda_{23}}{\lambda_{12}\lambda_{21} - \lambda_{11}\lambda_{22}} \quad (22b)$$

$$\lambda_T = \frac{\lambda_{21}\lambda_{14}}{\lambda_{12}\lambda_{21} - \lambda_{11}\lambda_{22}} \quad (22c)$$

$$B^* = \frac{1}{(r_2^2 - r_1^2)\cosh r_1(L-l)}\{(r_2^2 - \lambda_{22})\sigma_{m1}^1 - \lambda_{21}\sigma_f^1 + [\lambda_f - \lambda_m(r_2^2 - \lambda_{22})]\sigma - r_2^2\lambda_T\sigma^T\} \quad (22d)$$

$$D^* = \frac{1}{(r_1^2 - r_2^2)\cosh r_2(L-l)}\{(r_1^2 - \lambda_{22})\sigma_{m1}^1 - \lambda_{21}\sigma_f^1 + [\lambda_f - \lambda_m(r_1^2 - \lambda_{22})]\sigma - r_1^2\lambda_T\sigma^T\} \quad (22e)$$

where σ_f^1 and σ_{m1}^1 are the axial stresses at the boundary between the bonded and debonded region, i.e. $\sigma_f^1 = \sigma_f^z(L-l)$, $\sigma_{m1}^1 = \sigma_{m1}^z(L-l)$ and can be obtained from Equations 16a and b.

2.2. Fracture mechanics analysis of matrix cracking and interface debonding.

The minimum fracture stress criterion is used to describe the competition between matrix cracking and interface debonding. The strain energy release rate, G, can be calculated by differentiating the total elastic energy, U, with respect to the area of crack surface, s

$$G = \frac{\partial U}{\partial s} \quad (23)$$

For a linear elastic system, U can be calculated from

$$U = \frac{1}{2E}\iiint_V \{(\sigma^z)^2 + (\sigma^r)^2 + (\sigma^\theta)^2 - 2\nu(\sigma^z\sigma^r + \sigma^z\sigma^\theta + \sigma^r\sigma^\theta) + 2(1+\nu)[(\tau^{rz})^2 + (\tau^{z\theta})^2 + (\tau^{r\theta})^2]\}\,dV \quad (24)$$

In this case, U can be written as

$$\begin{aligned} U = \int_0^{2\pi}\int_0^L \Bigg\{ & \frac{1}{E_f}\int_0^a [(\sigma_f^z)^2 + (\sigma_f^r)^2 + (\sigma_f^\theta)^2 - 2\nu_f(\sigma_f^z\sigma_f^r + \sigma_f^z\sigma_f^\theta + \sigma_f^r\sigma_f^\theta)]\,r\,dr \\ & + \frac{1}{E_m}\int_a^b [(\sigma_{m2}^z)^2 + (\sigma_{m2}^r)^2 + (\sigma_{m2}^\theta)^2 - 2\nu_m(\sigma_{m2}^z\sigma_{m2}^r + \sigma_{m2}^z\sigma_{m2}^\theta + \sigma_{m2}^r\sigma_{m2}^\theta) + 2(1+\nu_m)(\tau_{m2}^{rz})^2]\,r\,dr \\ & + \frac{1}{E_m}\int_b^R [(\sigma_{m1}^z)^2 + (\sigma_{m1}^r)^2 + (\sigma_{m1}^\theta)^2 - 2\nu_m(\sigma_{m1}^z\sigma_{m1}^r + \sigma_{m1}^z\sigma_{m1}^\theta + \sigma_{m1}^r\sigma_{m1}^\theta) + 2(1+\nu_m)(\tau_{m1}^{rz})^2]\,r\,dr \Bigg\}\,dz\,d\theta \end{aligned} \quad (25)$$

in which σ_{m2}^z, τ_{m1}^{rz} and τ_{m2}^{rz} can be obtained by combining Equations 5a–c, 7a, b, 11 and 16a, b and 19a,b. σ_{m1}^r, σ_{m1}^θ and σ_{m2}^r, σ_{m2}^θ can be solved from Appendix A.

In fibre fragmentation tests, a matrix crack of initial size b may initiate immediately after the fibre breaks. Prior to interface debonding, the strain energy release rate, G_b, for the matrix crack can be obtained from Equations 23 and 25, with $s = \pi(b^2 - a^2)$, i.e.

$$G_b = \frac{1}{2\pi b}\left(\frac{\partial U}{\partial b}\right)_{l=0} \quad (26)$$

With the interface debond ($s = 4\pi al$), the strain energy release rate for interface debonding G_l is [15]

$$G_l = \frac{1}{4\pi a}\left(\frac{\partial U}{\partial l}\right)_{l\to 0} \quad (27)$$

where the debond length l approaches zero is used to describe the initiation of interface debonding.

If G_b^c and G_l^c are used to represent the specific fracture resistances of the matrix and interface, respectively, as the applied stress is increased, both the strain energy release rates for the matrix crack, G_b, and the interfacial crack, G_l, increase. For a given applied stress σ_a, when $G_b \geqslant G_b^c$, the matrix crack propagates outwards leading to matrix fracture. But if $G_b < G_b^c$ and $G_l \geqslant G_l^c$, there is no matrix cracking, an interface debond occurs and propagates along the interface from the broken end of the fibre. Substituting the stress components determined in the previous section into Equations 25–27, the strain energy release rates for both matrix crack, G_b, and interface debond, G_l, can be obtained. Whether matrix cracking or interface debonding occurs first can be determined by comparing the strain energy release rates with the corresponding fracture resistances at any given applied stress, σ_a, which is equivalent to the minimum fracture stress criterion [16].

3. Numerical examples and discussion

Numerical results are calculated for a carbon fibre/epoxy matrix system, of which the elastic properties of the constituents and the interfacial properties are given in Table I. The length of the fibre fragment is taken as 1 mm (longer or shorter fragment lengths can be used in these numerical examples provided that they are larger than the saturation CTL. In the carbon fibre/epoxy composite chosen the CTL is about 0.5 mm [6]). In all the figures shown, the ratio of the matrix crack radius to the fibre radius b/a is used as a dimensionless matrix crack radius.

The variation of fibre axial stress and interfacial shear stress is plotted as a function of the axial distance along the fibre in Fig. 3a and b. The applied stress is fixed at $\sigma_a = 0.1$ GPa. The stress distributions are only given for the half length of the fragment because the stresses are symmetrical about the plane $z = 0$. In both figures the interface is fully bonded and the curve $b/a = 1$ represents the condition of no matrix crack. It can be clearly seen that the stress distributions are highly dependent on the matrix crack

TABLE I Fibre, matrix and interface characteristics [6, 17] and $\Delta T = -100\,^{\circ}C$

Fibre	Young's modulus, E_f(GPa)	230
	Poisson's ratio, ν_f	0.2
	Radius, a (mm)	0.003
	Thermal expansion coefficient, $\alpha_f^T(10^{-6}\,^{\circ}C^{-1})$	−0.99
Matrix	Young's modulus, E_m(GPA)	3
	Poisson's ratio, ν_m	0.4
	Radius, R (mm)	2.5
	Thermal expansion coefficient, $\alpha_m^T(10^{-6}\,^{\circ}C^{-1})$	65
	Fracture resistance, $G_b^c\,(J\,m^{-2})$	500
Interface	Residual clamping stress, q_0 (MPa)	−8.4
	Frictional coefficient, μ	0.8
	Fracture resistance, $G_l^c\,(J\,m^{-2})$	13

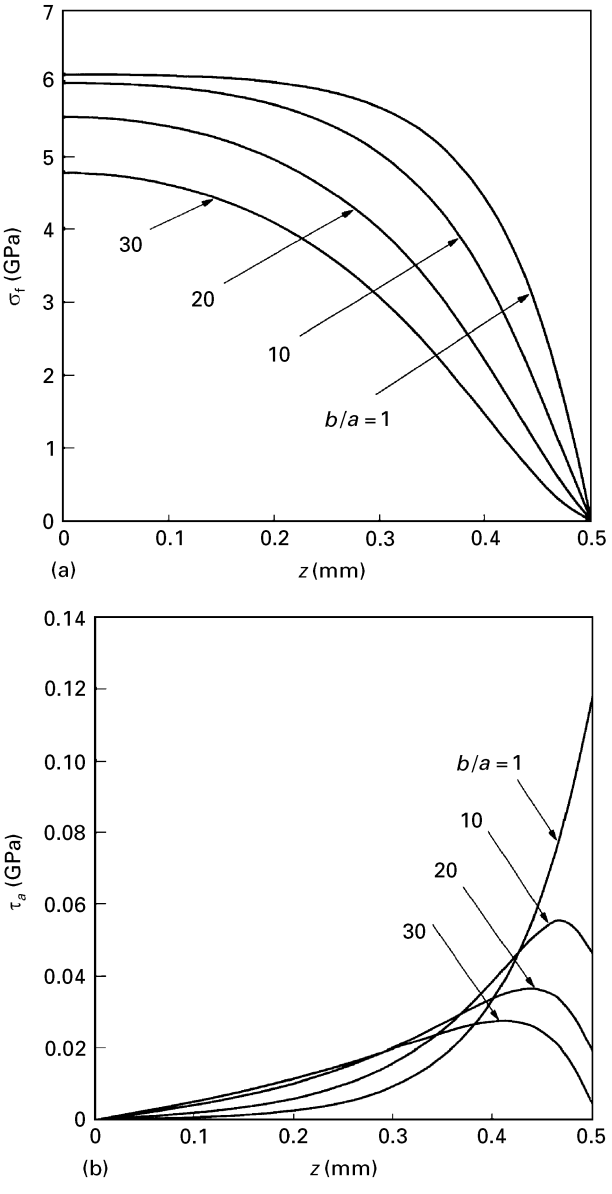

Figure 3 The distributions of (a) fibre axial stress, σ_f^z, (b) interfacial shear stress, τ_a, in the half-fragment. The ratio b/a denotes the dimensionless matrix crack radius. $\sigma_a = 0.1$ GPa.

radius. When the matrix crack radius increases, the maximum values of both fibre axial stress and interfacial shear stress decrease. In Fig. 4, the maximum fibre axial stress, $\sigma_{f,max}$, is given as a function of the fibre length, where the dimensionless matrix crack

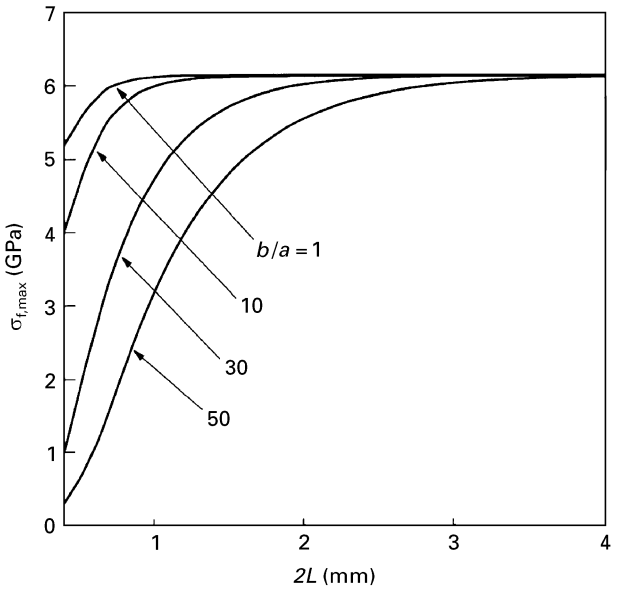

Figure 4 The maximum fibre axial $\sigma_{f,max}$ as a function of the fibre fragment length for different matrix crack radius b/a. $\sigma_a = 0.1$ GPa.

radii are 1, 10 30 and 50. For each case, $\sigma_{f,max}$ decreases with the matrix crack radius. The fibre breaks when the maximum fibre axial stress reaches the fibre tensile strength, σ_{TS}. So if a large matrix crack appears after fibre breakage, a greater applied stress is required to cause a new fibre break. Because the matrix cracks appear at the ends of the fragment, as shown in Fig. 4, for the shorter fibre fragment, the effect of matrix crack on the maximum fibre axial stress is more significant. From Figs 3a, b and 4, it is found that in the fibre fragmentation test, a matrix crack which is initiated by a fibre break can reduce the efficiency of stress transfer from the matrix to the fibre, and consequently, affect the behaviour of subsequent fibre breaks.

The strain energy release rates of the matrix crack, G_b, and the interface crack, G_l, as a function of applied stress, σ_a, are shown in Fig. 5a and b. In these figures, G_b and G_l are significantly dependent on the radius of the matrix crack. However, G_b increases but G_l decreases with b/a at any given applied stress. By the theory of fracture mechanics, crack propagation occurs when its strain energy release rate exceeds the specific fracture resistance. In this work, the specific fracture resistances of the matrix, G_b^c, and interface, G_l^c, are assumed to be $500\,J\,m^{-2}$ [17] and $13\,J\,m^{-2}$ [6], respectively. The competition between matrix cracking and interface debonding is shown in Fig. 6a–c where $\sigma_{a,ip}$, $\sigma_{a,mp}$ are the applied stress level corresponding to interface debonding and matrix cracking, respectively. From Fig. 6a, in which $E_m = 3$ GPa, $a = 0.003$ and 0.03 mm, it is shown that $\sigma_{a,mp}$ decreases but $\sigma_{a,ip}$ increases with increasing matrix crack size. For the fibre of radius 0.003 mm, when the ratio b/a is smaller than 15, the applied stress required for interface debond initiation, $\sigma_{a,ip}$, is smaller than that for matrix cracking, $\sigma_{a,mp}$. Hence, interface debonding occurs before the matrix crack propagates. However, for $b/a > 15$, $\sigma_{a,mp}$ is smaller than $\sigma_{a,ip}$, matrix fracture therefore occurs before interface debonding. For the large fibre of radius 0.03 mm,

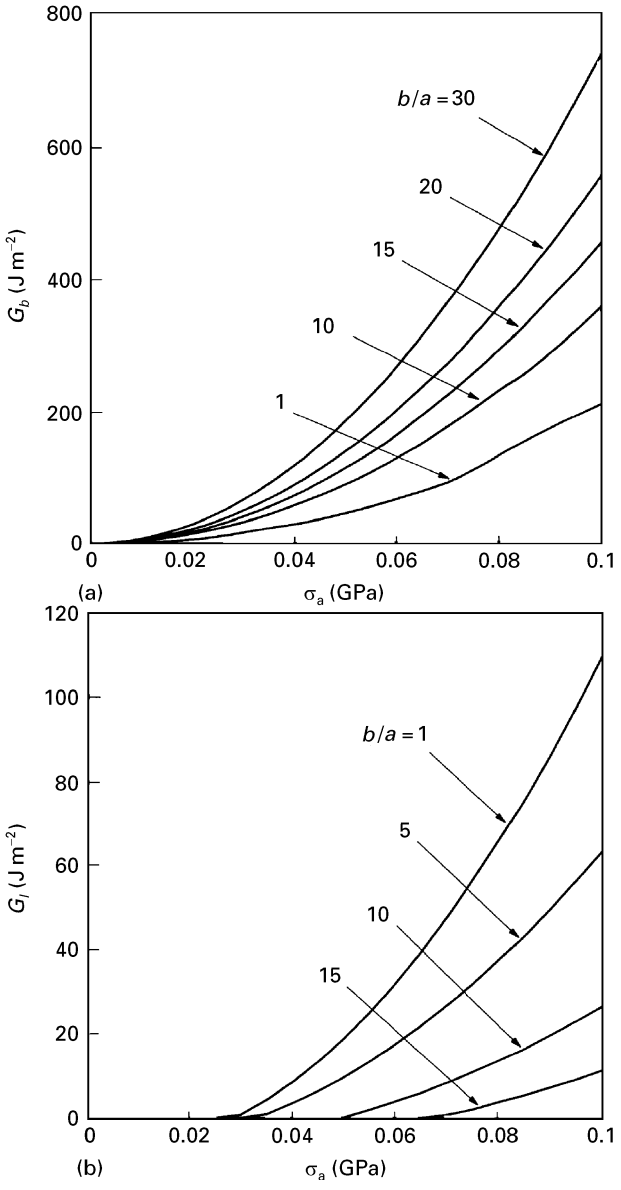

Figure 5 Strain energy release rate of (a) matrix crack G_b, and (b) interface crack G_l versus applied stress σ_a for different radius of matrix crack b/a. In (a), curve $b/a = 1$ represents the case in which the initial matrix crack size is very small, i.e. b approaches a.

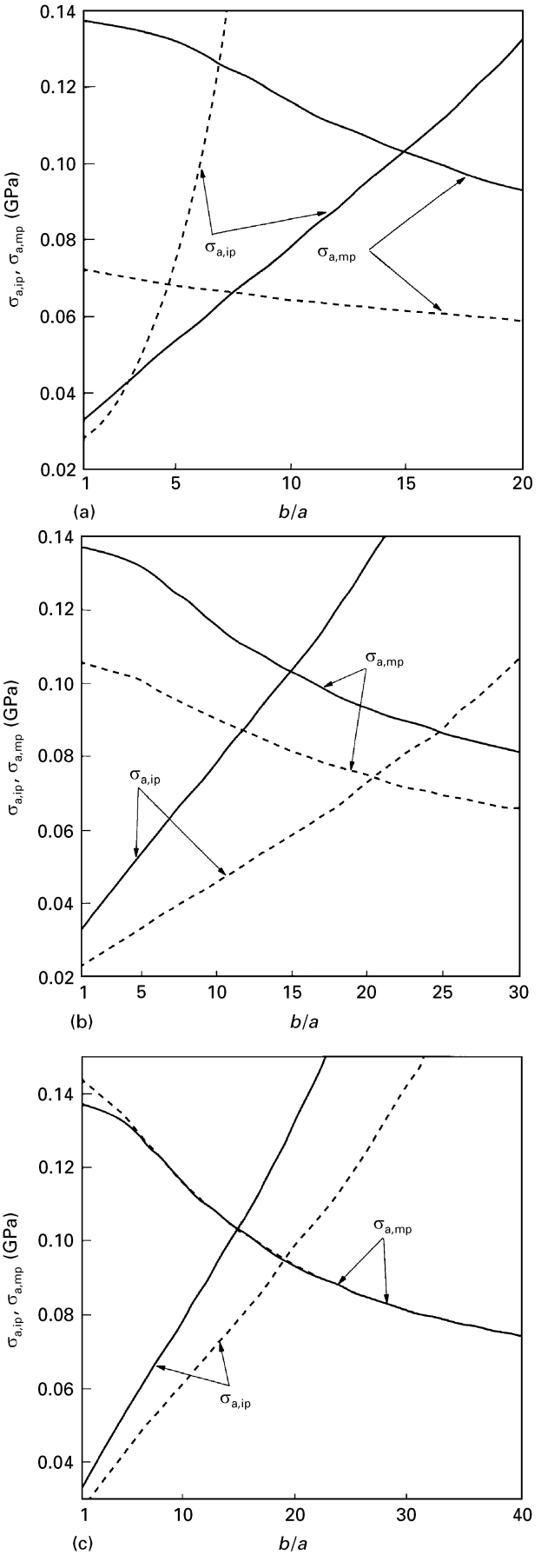

Figure 6 The applied stress levels corresponding to interface debonding $\sigma_{a,ip}$ and matrix cracking $\sigma_{a,mp}$ as a function of the dimensionless matrix crack radius b/a for three cases: (a) $a =$ (——) 0.003 and (– – –) 0.03 mm, and $E_m = 3$ GPa; (b) $a = 0.003$ mm, $E_m =$ (– – –) 2 and (——) 3 GPa; and (c) $a = 0.003$ mm, $E_m = 3$ GPa, (——) with residual thermal stress ($\Delta T = -100\,^{\circ}C$) and (– – –) without residual thermal stress.

when $b/a < 4.5$, $\sigma_{a,ip} < \sigma_{a,mp}$, interface debonding occurs first. But for $b/a > 4.5$, $\sigma_{a,ip} > \sigma_{a,mp}$, matrix cracking commences before interface debonding. Fig. 6b shows the competition between matrix cracking and interface debonding for a softer matrix resin, $E_m = 2$ GPa. If $b/a < 21$, $\sigma_{a,ip} < \sigma_{a,mp}$, interface debonding occurs first, and when $b/a > 21$, matrix crack propagates before interface debonding. Fig. 6a and b show that the transition b/a ratio from interface debonding to matrix cracking is determined by geometrical and material parameters of the fibre and matrix resin. As shown by Gent and Wang [12, 13], and in Fig. 6a, for very large radius of the fibre, matrix cracking may be the only failure mode with no interface debonding. (For example, if $a = 0.15$ mm $\sigma_{a,ip}$ is always higher than $\sigma_{a,mp}$ even if b/a approaches 1.) The effect of residual thermal stress on the competition between matrix cracking and interface debonding is shown in Fig. 6c. Residual thermal stress increases $\sigma_{a,ip}$ but it has no effect on $\sigma_{a,mp}$. Consequently, the

transition of the b/a ratio from interface debonding to matrix cracking is increased from 15 to 19.5 in the absence of any residual thermal stress. Residual thermal stress therefore reduces the strain energy release rate for interface debonding and alters the competition between matrix cracking and interface debonding.

The numerical examples presented above in Figs 4–6 are only concerned with the competition of matrix cracking and interface debonding when a matrix crack of a given size is known. In this paper we have not yet shown how the mean fragment length at saturation is affected. To do this, we need to extend the theoretical analysis on the applied stress required to continue the interface debonding and compare it with that required for fibre fragment fracture and that for matrix cracking. Interpretation of the experimental data from fibre fragmentation tests to extract fibre–matrix interface properties is not as straight forward, in the presence of matrix cracking and interface debonding, as previous models and methods imply [1–5]. This problem will be dealt with in a future paper.

It is noted that, in the model given in this paper, the outer cylindrical surface of the matrix ($r = R$) is only considered as a free boundary ($\sigma_m^r(r = R) = 0$, $\tau_m^{rz}(r = R) = 0$), which corresponds to the single fibre/matrix composite model. In the case of an aligned fibre-reinforced composite, because the outer cylindrical surface is constrained by the neighbouring fibres, the boundary conditions are given by $u_m^r(r = R) = 0$, and $\tau_m^{rz}(r = R) = 0$. Substituting the boundary condition $u_m^r(r = R) = 0$ for $\sigma_m^r(r = R) = 0$ in Equation A16 (Appendix A), the coefficients k'_{ij} can be solved. Replacing k_{ij} by k'_{ij} in the coefficients η_{ij}, λ_{ij} (Appendices B and C) and q^*, the solutions of the stress components obtained in Section 2.1 are also available for the case of an aligned fibre-reinforced composite.

4. Conclusion

A theoretical analysis of the effect of matrix crack on the fibre fragmentation test has been presented. The competition between matrix cracking and interface debonding is controlled by the minimum fracture stress criterion. It is shown that the matrix crack radius has a significant influence on the strain energy release rates for both the matrix crack, G_b, and the interface crack, G_l. Therefore, it is one of the most important factors which control the failure mode in a fibre fragmentation test. Additionally, the radius of the fibre, the Young's modulus of the matrix and the residual thermal stress have remarkable effects on the competition between matrix cracking and interface debonding.

The results of the fibre axial stress and interface shear stress distributions show that the matrix crack can reduce substantially the efficiency of stress transfer from the matrix to the fibre. Therefore, the presence of matrix cracks initiated by fibre breaks will greatly affect the fibre fragmentation behaviour and complicate the evaluation of the fibre/matrix interface properties.

Acknowledgements

The authors thank the Australian Research Council (ARC) for the continuing support of this project. H.-Y. Liu was supported by a Postgraduate Scholarship and L.-M. Zhou by a Postdoctoral Fellowship, both funded by the ARC.

Appendix A. Coefficients k_{ij}

In a single fibre/matrix system considered in Fig. 2, both the material structure and the applied load are symmetrical about the z-axis. The stresses and displacements in each cylinder are given by [15]

$$\sigma_f^r = \sigma_f^\theta = A \tag{A1}$$

$$u_f^r = \frac{1-\nu_f}{E_f} Ar - \frac{\nu_f}{E_f}\sigma_f^z r \tag{A2}$$

$$\sigma_{m2}^r = \frac{B}{r^2} + C \tag{A3}$$

$$\sigma_{m2}^\theta = -\frac{B}{r^2} + C \tag{A4}$$

$$U_{m2}^r = -\frac{1}{E_m}\left[\frac{1+\nu_m}{r}B - (1-\nu_m)Cr\right] - \frac{\nu_m}{E_m}\sigma_{m2}^z r \tag{A5}$$

$$\sigma_{m1}^r = \frac{D}{r^2} + E \tag{A6}$$

$$\sigma_{m1}^\theta = \frac{D}{r^2} + E \tag{A7}$$

$$u_{m1}^r = -\frac{1}{E_m}\left[\frac{1+\nu_m}{r}D - (1-\nu_m)Er\right] - \frac{\nu_m}{E_m}\sigma_{m1}^z r \tag{A8}$$

where A, B, C, D and E are stress parameters to be determined. The continuity conditions of stresses and displacements of each cylinder at the interface and the boundary conditions at the outer surface of the matrix are

$$\sigma_f^r(a, z) = \sigma_{m2}^r(a, z) \tag{A9}$$

$$\sigma_{m2}^r(b, z) = \sigma_{m1}^r(b, z) \tag{A10}$$

$$\sigma_{m1}^r(R, z) = 0 \tag{A11}$$

$$u_f^r(a, z) = u_{m2}^r(a, z) \tag{A12}$$

$$u_{m2}^r(b, z) = u_{m1}^r(b, z) \tag{A13}$$

So we can obtain

$$A = k_{1A}\sigma_f^z + k_{2A}\sigma_{m1}^z + k_{3A}\sigma_{m2}^z \tag{A14}$$

$$B = k_{1B}\sigma_f^z + k_{2B}\sigma_{m1}^z + k_{3B}\sigma_{m2}^z \tag{A15}$$

$$C = k_{1C}\sigma_f^z + k_{2C}\sigma_{m1}^z + k_{3C}\sigma_{m2}^z \tag{A16}$$

$$D = k_{1D}\sigma_f^z + k_{2D}\sigma_{m1} + k_{3D}\sigma_{m2} \tag{A17}$$

$$E = k_{1E}\sigma_f^z + k_{2E}\sigma_{m1}^z + k_{3E}\sigma_{m2}^z \tag{A18}$$

where

$$k_{1C} = \frac{\alpha \nu_f}{\delta} \tag{A19}$$

$$k_{2C} = \frac{b^2 \nu_m [\alpha(1-\nu_f)+1+\nu_m]}{2a^2 \gamma_1 \delta} \tag{A20}$$

$$k_{3C} = -\frac{\nu_m}{\delta}\left\{1+\frac{b^2[\alpha(1+\nu_f)+1+\nu_m]}{2a^2\gamma_1}\right\} \tag{A21}$$

$$k_{1B} = -\frac{b^2(1+\gamma_1)k_{1C}}{\gamma_1} \tag{A22}$$

$$k_{2B} = -\frac{b^2[\nu_m+2(1+\gamma_1)k_{2C}]}{2\gamma_1} \tag{A23}$$

$$k_{3B} = \frac{b^2[\nu_m-2(1+\gamma_1)k_{3C}]}{2\gamma_1} \tag{A24}$$

$$k_{iA} = \frac{k_{iB}}{a^2}+k_{iC} \qquad (i=1,2,3) \tag{A25}$$

$$k_{iD} = R^2\gamma_1\left(\frac{k_{iB}}{b^2}+k_{iC}\right) \qquad (i=1,2,3) \tag{A26}$$

$$k_{iE} = -\gamma_1\left(\frac{k_{iB}}{b^2}+k_{iC}\right) \qquad (i=1,2,3) \tag{A27}$$

$$\gamma_1 = \frac{b^2}{R^2-b^2} \tag{A28}$$

$$\delta = -\frac{(R^2-a^2)[\alpha(1-\nu_f)+1+\nu_m]+2a^2}{a^2} \tag{A29}$$

Appendix B. Coefficients η_{ij}

$$\eta_{11} = \frac{2\mu}{a}\left(k_{1A}-\frac{a^2k_{3A}}{b^2-a^2}\right) \tag{A30}$$

$$\eta_{12} = \frac{2\mu}{a}\left(k_{2A}-\frac{R^2-b^2}{b^2-a^2}k_{3A}\right) \tag{A31}$$

$$\eta_{13} = \frac{2\mu}{a}\frac{R^2-b^2}{b^2-a^2}k_{3A} \tag{A32}$$

$$\eta_{21} = -\frac{a^2}{(b^2-a^2)\delta_1}(\nu_m^2-1) \tag{A33}$$

$$\eta_{22} = \frac{R^2-a^2}{(b^2-a^2)\delta_1}(1-\nu_m^2) \tag{A34}$$

$$\eta_{23} = \frac{R^2-b^2}{(b^2-a^2)\delta_1}(\nu_m^2-1) \tag{A35}$$

where

$$\delta_1 = (1+\nu_m)\left(R^2\ln\frac{R}{b}-\frac{R^2-b^2}{2}\right) \tag{A36}$$

In all calculations, η_{21} is much smaller than the others. It is reasonable to neglect η_{21} in equation 14b to simplify the solution.

Appendix C. Coefficients λ_{ij} and r_1, r_2

$$\lambda_{11} = \delta_2\left\{\alpha+2(\nu_m k_{1C}-\alpha\nu_f k_{1A}) + \frac{a^2}{b^2-a^2}[1-2(\nu_m k_{3C}-\alpha\nu_f k_{3A}) - \delta_3(1-\nu_m^2)]\right\} \tag{A37}$$

$$\lambda_{12} = \delta_2\left\{2(\nu_m k_{2C}-\alpha\nu_f k_{2A}) + \frac{R^2-b^2}{b^2-a^2}[1-2(\nu_m k_{3C}-\alpha\nu_f k_{3A})] - \delta_3(1-\nu_m^2)\frac{R^2-a^2}{b^2-a^2}\right\} \tag{A38}$$

$$\lambda_{13} = -\delta_2\frac{R^2-b^2}{b^2-a^2}[1-2(\nu_m k_{3C}-\alpha\nu_f k_{3A}) - \delta_3(1-\nu_m^2)] \tag{A39}$$

$$\lambda_{14} = \delta_2 \tag{A40}$$

$$\lambda_{2j} = \eta_{2j} \qquad (j=1,2,3) \tag{A41}$$

where η_{2j} are given in Appendix B, and

$$\delta_2 = \frac{b^2-a^2}{(1+\nu_m)a^2\left(b^2\ln\frac{b}{a}-\frac{b^2-a^2}{2}\right)} \tag{A42}$$

$$\delta_3 = \frac{R^2-b^2}{b^2-a^2}\frac{a^2\ln\frac{b}{a}-\frac{b^2-a^2}{2}}{R^2\ln\frac{R}{b}-\frac{R^2-b^2}{2}} \tag{A43}$$

Combining Equations 19a and b yields a fourth order linear differential equation

$$\frac{d^4\sigma_{m1}^z}{dz^4}-(\lambda_{11}+\lambda_{22})\frac{d^2\sigma_{m1}^z}{dz^2}-(\lambda_{12}\lambda_{21}-\lambda_{11}\lambda_{22})\sigma_{m1}^z = (\lambda_{21}\lambda_{13}-\lambda_{11}\lambda_{23})\sigma-\lambda_{21}\lambda_{14}\sigma^T \tag{A44}$$

From the boundary condition $\sigma_{m1}^z(\pm(L-l))=\sigma_{m1}^l$, the solution of Equation A44 is

$$\sigma_{m1}^z = B^*\cosh r_1 z + D^*\cosh r_2 z - \frac{\lambda_{21}\lambda_{13}-\lambda_{11}\lambda_{23}}{\lambda_{21}\lambda_{12}-\lambda_{11}\lambda_{22}}\sigma+\frac{\lambda_{21}\lambda_{14}}{\lambda_{21}\lambda_{12}-\lambda_{11}\lambda_{12}}\sigma^T \tag{A45}$$

in which

$$r_1 = \left\{\frac{\lambda_{11}+\lambda_{22}+[(\lambda_{11}+\lambda_{22})^2+4\lambda_{12}\lambda_{21}-4\lambda_{11}\lambda_{22}]^{1/2}}{2}\right\}^{1/2} \tag{A46}$$

$$r_2 = \left\{\frac{\lambda_{11}+\lambda_{22}-[(\lambda_{11}+\lambda_{22})^2+4\lambda_{12}\lambda_{21}-4\lambda_{11}\lambda_{22}]^{1/2}}{2}\right\}^{1/2} \tag{A47}$$

B^* and D^* are given by Equation 22a and b respectively. It should be mentioned that r_1 and r_2 are real

values, which hold for all calculations in this paper. If, in some other cases, the values of r_1 and r_2 are imaginary, the solution of Equation A44 will be different.

References

1. A. KELLY and W. R. TYSON, *J. Mech. Phys. Solids* **13** (1965) 329.
2. T. OHSAWA, A. NAKAYAMA, M. MIWA and A. HASEGAWA, *J. Appl. Polym. Sci.* **22** (1978) 3203.
3. A. N. NETRAVALI, L. T. T. TOPOLESKI, W. H. SACHSE and S. L. PHOENIX, *Compos. Sci. Technol.* **35** (1989) 13.
4. R. B. HENSTENBURG and S. L. PHOENIX, *Polym. Compos.* **10** (1989) 389.
5. TH. LACROIX, B. TILMANS, R. KEUNINGS, M. DESAEGER and I. VERPOEST, *Compos. Sci. Technol.* **43** (1992) 379.
6. L. M. ZHOU, J. K. KIM, C. BAILLIE and Y.-W. MAI, *J. Compos. Mater.* **29** (1995) 881.
7. H. Y. LIU, Y. W. MAI, L. M. ZHOU and L. YE. *Compos. Sci. Technol.* **52** (1994) 253.
8. J. MULLIN, J. M. BERRY and A. GATTI. *J. Compos. Mater.* **2** (1968) 82.
9. A. N. NETRAVALI and P. SCHWARTZ. *Polym. Compos.* **10** (1989) 385.
10. P. FEILLARD, G. DESARMOT and J. P. FAVRE, *Compos. Sci. Technol.* **49** (1993) 109.
11. *Idem*, *ibid.* **50** (1994) 265.
12. A. N. GENT and C. WANG, *J. Mater. Sci.* **27** (1992) 2539.
13. *Idem*, *ibid.* **28** (1993) 2494.
14. H. Y. LIU, L. M. ZHOU, Y. W. MAI and L. YE, *Key Eng. Mater.* **116/7** (1996) 121.
15. Y. C. GAO, Y.-W. MAI and B. COTTERELL, *J. Appl. Math. Phys.* (*ZAMP*) **39** (1989) 550.
16. A. G. ATKINS and Y.-W. MAI, "Elastic and Plastic Fracture-Metals, Polymers, Composites, Ceramics, Biological Materials" (Ellis Horwood/John Wiley, 1985).
17. N. P. CHEREMISINOFF, "Handbook of Ceramics and Composites", Vol. 2 (Marcel Dekker, New York, 1992).

Received 6 February
and accepted 18 March 1996